Available online at www.sciencedirect.com
SCIENCE DIRECT
International Journal of Mass Spectrometry 248 (2006) 124–135
International Journal of Mass Spectrometry
www.elsevier.com/locate/ijms

Prediction of N–C_α bond cleavage frequencies in electron capture dissociation of Trp-cage dications by force-field molecular dynamics simulations

Alexandra Patriksson [b], Christopher Adams [a], Frank Kjeldsen [a], Johan Raber [b], David van der Spoel [b], Roman A. Zubarev [a,*]

[a] *Laboratory for Biological and Medical Mass Spectrometry, Division of Ion Physics, Uppsala University, Uppsala, Sweden*
[b] *Institute for Cell and Molecular Biology, Division of Molecular BioPhysics, Uppsala University, Uppsala, Sweden*

Received 6 October 2005; received in revised form 12 November 2005; accepted 14 November 2005
Available online 27 December 2005

Abstract

Fragment ion abundances observed in electron capture dissociation (ECD) of dications of four stereoisomers (all-L, D-Tyr[3], D-Gln[5] and D-Leu[7]) of the Trp-cage protein correlated with the charge solvation patterns produced by molecular dynamics simulations (MDS) of the corresponding gas-phase structures. The degree of the correlation was however insufficient to distinguish the correct stereoisomers or make quantitative predictions. Much higher correlation was found between the ECD patterns and the frequencies of occurrence of neutral H-bonds to the carbonyls of the fragmenting amides. Based on this finding, a new ECD mechanism is suggested for N–C_α bond breakage, in which low-energy electrons are captured on a neutral hydrogen bond, with subsequent hydrogen atom transfer to the backbone carbonyl forming labile aminoketyl radical that rapidly fragments through α-cleavage. The neutral H-bonding model quantitatively predicted the ECD patterns of all four stereoisomers and correctly recognized them from the experimental data by comparing them to MDS results. The predictive power of the neutral H-bonding model may help in the future to solve gas-phase protein structures.

Keywords: Electron capture dissociation; Fragmentation; Polypeptides; Hydrogen transfer; Gas-phase structure

1. Introduction

Electron capture dissociation (ECD) is a dissociative recombination reaction between multiply charged, gas-phase polypeptides and low-energy electrons [1]. The polycations are typically produced by electrospray ionization [2], while the low-energy electrons can either be free [1] or bound to an anion [3] or to an atom with low ionization energy [4–6]. ECD specifically cleaves certain strong bonds, of which N–C_α backbone bond cleavage that leads to c and z fragment formation is of a particular interest for applications in protein analysis and proteomics [7–10]. The mechanism of ECD is currently widely debated, with plausible hypotheses ranging from the direct electron action [11] to a Coulomb-assisted electron attachment to the backbone carbonyls [12] to an action through an intermediate hydrogen atom [13] or a radical cascade [14]. In the first two mechanisms, electron capture occurs on the excited state of a backbone carbonyl. Since such a capture is by 2.5 eV endothermic [12], the cleavage must occur in the vicinity of a positive charge. In contrast, the hydrogen-atom and radical cascade mechanisms allow for charge-remote cleavage [13,14], although the proximity to a charge and thus shorter $H^\bullet$ transfer distances should increase the cleavage probability.

There are currently two main approaches to studying the ECD mechanism. The first approach involves detailed quantum-mechanical considerations of small model systems [12,13,15–17]. The alternative strategy is to reproduce global phenomena using a combination of experimental results and semi-empirical molecular dynamics simulations (MDS) [18–20]. These two approaches are complementary. The experimental results alone yield mere clues, the force-field MDS can reveal only coarse mechanistic details, while detailed ab initio

* Corresponding author. Tel.: +46 18 471 72 09; fax: +46 18 471 72 09.
E-mail address: roman.zubarev@bmms.uu.se (R.A. Zubarev).

1387-3806/$ – see front matter © 2005 Elsevier B.V. All rights reserved.
doi:10.1016/j.ijms.2005.11.018

simulations provide precious insights but are currently limited to small systems.

The ultimate challenge for an ECD model is to explain and predict the relative abundances of N–C_α bond cleavages. The first systematic attempt to correlate experimental ECD data with MDS results based on charge-solvation model has been made by Polfer et al. [19,20]. In extensive simulations performed on 10–12 residue long peptide dications, they obtained qualitative similarity, but no quantitative correlation of N–C_α cleavage frequencies with charge solvation patterns was demonstrated. These studies highlighted the two main obstacles in predicting ECD cleavage frequencies directly from the MDS results. The first difficulty is the vast multitude of possible conformations of the polypeptide chain in vacuum (although in solution this number may be even larger), which are very difficult to sample within a reasonable simulation time. The second challenge to establish the location of the positive charges on the molecule and the probability for each charge to be neutralized.

The first problem can be avoided by choosing polypeptides with more or less defined gas-phase structures which do not change significantly on the experimental and simulation time scales. For this purpose, small peptides appear to be far too flexible; they may interconvert fast between the multiple potential energy minima. Proteins can retain one dominant, fairly compact conformation in the gas phase provided they are not excessively charged or vibrationally excited [21]. However, such low-charged, cool proteins are difficult to fragment by ECD [22], while highly protonated proteins tend to be unfolded [23,24]. Fortunately, the smallest known protein Trp-cage [25] is only 20 residues long, and its dications have in the gas phase a compact conformation [26]. In solution at pH 7, Arg^{16} and Lys^8 of Trp-cage are protonated and Asp^9 is deprotonated, but in the gas-phase dications all experimental evidence supports protonation of Gln^5 and Arg^{16} residues, and no evidence is present for a zwitterionic structure [26]. In ECD, the Gln-located charge is neutralized preferentially because of its lower basicity, while the Arg-located proton acts as a spectator [26], giving rise to a series of C-terminal z ions from z_{15} to z_{19}. The abundances of these ions can be used for comparison with MDS results, but five abundances constitute too small a dataset for a statistically valid comparison. Extending the study to other molecule is undesirable, first because of the lack of small, well-characterized proteins, and second because their structures may be too disparate for meaningful comparison. Thus in the current study Trp-cage was complemented with its mutants obtained by the most subtle of all modifications, conversion of the chirality of a single amino acid [27]. It has been shown earlier that dications of the D-Tyr^3 stereoisomer of Trp-cage give distinctly different ECD mass spectra than the all-L form [26]. The two other stereoisomers used in this work were the D-Gln^5 and D-Leu^7 molecules, which also give different ECD patterns [28]. The Gln_5 residue is protonated in the all-L and D-Tyr^3 forms [26], and was expected to be protonated in D-Gln^5 and D-Leu^7 stereoisomers as well. Thus stereo-conversion of this residue was expected to markedly change the charge solvation pattern. The Leu^7 residue is also structurally important because of its location near the inner part of the sequence.

2. Materials and methods

2.1. Polypeptide synthesis

Trp-cage proteins (NLYIQWLKDGGPSSGRPPPS) were synthesized in house using solid-phase Fmoc chemistry with an Applied Biosystems 431A (Foster City, CA) and Intavis AG ResPep (Gladbach, Germany) automatic peptide synthesizers. D-isomer amino acids were purchased from Novabiochem (Laufelfingen, Switzerland) and Cambridge Research Biochemicals Ltd. (Cleveland, UK). Molecules were further purified from truncated peptides and those with protecting groups still attached by reversed-phase HPLC using a Vydac C18 column (Hesperia, CA). Final purity was tested by MALDI TOF mass spectrometry.

2.2. Mass spectrometry

ECD experiments were performed using a 7 T LTQ FT mass spectrometer (Thermo, Bremen, Germany) equipped with a commercial ECD set-up. Peptides were dissolved in electrospray solvent consisting of water, methanol and acetic acid in proportions 49:49:2 (v/v) to a concentration of approximately 5 pmol/μL. To study the effect of solvent, two other solutions were used, 2 mM ammonium bicarbonate, a buffer used in many studies to promote "native" structure formation [21], and 100 μM quinhydrone, a redox reagent effectively diminishing the average charge state of electrosprayed proteins [29]. Peptides were electrosprayed by direct infusion using a Proxeon nanosource (Odense, Denmark) with applied voltages ranging from 700 to 1200 V. ECD was performed by 70 ms irradiation with <1 eV electrons. ECD of 3+ of all Trp-cage isomers was performed to check that each isomer was protonated at the Arg_{16} and Gln_5 residues, as described in ref. [26].

2.3. Molecular dynamics simulations

GROMACS program package was used for the simulations [30]. All simulations were performed in vacuum using OPLS-AA force field and the replica exchange approach at 16 different temperature points ranging from 275 to 419 K. Each simulation started from the "native" solution-phase structure determined by NMR [25], and lasted for 200 ns. Prior to the replica exchange run, an energy minimization was performed. To save the simulation time, bond lengths were constrained using the LINCS/SHAKE algorithm allowing the use of a time step of 2 fs [31]. Analyses of H-bonds were performed with the GROMOS96 program g_hbond. The position of the ionizing proton on Gln_5 (side-chain carbonyl oxygen) was determined by ab initio Gaussian proton affinity calculations. For control, one simulation was run for all-L isomer with the second (neutralized in ECD) proton located on the Lys^8 residue. For each isomer, temperature value and backbone carbonyl, at least three parameters were monitored: (A) the total number of time frames (sampled every picosecond) in which the protonated side chain (Gln^5 or Lys^8) was found to make a hydrogen bond with any other part of the protein, (B) for each frame, the total number of neutral hydrogen bonds established with the rest of the molecule, and

(C) the square-root deviation (RMSD) Δr of the global minimum gas-phase structure (see below) from the original "native" conformation. The first parameter represented a quantitative measure of the charge solvation probability, while Δr was used to estimate the degree of unfolding in the gas phase. Hydrogen bonds were defined using a geometrical criterion based on the donor–hydrogen–acceptor angle and the hydrogen–acceptor distance. As donor groups, OH and NH were considered. The 30° cutoff was chosen for the angle and 0.35 nm cutoff for the distance, in accordance with the first minimum of the radial distribution function of SPC-water.

The "global" minimum-energy structures of each stereoisomer were calculated as follows. First, a PCA analysis was performed on the coordinates of the trajectories to extract the major motions of the protein during the whole simulation. Then, the first two principal components, which usually contain most of the total covariance (total motional information) of the system, were taken to produce a 2D histogram. Assuming the system was in the state of thermodynamic equilibrium, the histogram was divided in 32 × 32 bins, and a free energy estimate was calculated for each bin as $W_i = -RT\ln(P_i)$, where P_i is the probability of finding a structure in bin i. One of the structures in the bin with the lowest W_i value was taken as the global minimum-energy structure. To accurately reflect the deviation from the solution-phase structure, the structure selected as the global minimum had to have the Δr value close to the computed average over the whole minimum-energy bin.

2.4. Comparative data analysis

To quantify the degree of overlap between the experimental data and theoretical predictions of MDS, the same product-moment correlation analysis was employed as in the previous studies [26,28]. In order to evaluate the statistical validity of the correlation factor r, model probability distributions were created by 10 million Monte Carlo simulations in which the N experimental datapoints (N = 4, 5 and 20) were correlated with N numbers randomly chosen between 0 and 1 or between −1 and 1, depending upon the maximum theoretical range of values assumed by the experimental datapoints. The threshold r_0 value corresponded to the 5% probability of obtaining this correlation value by randomly chosen datapoints.

Table 1
Normalized abundances of z_{15}, . . ., z_{19} ions in ECD mass spectra in Fig. 1

Fragment ion	all-L	D-Tyr[3]	D-Gln[5]	D-Leu[7]
z_{19}	1.000	0.407	0.877	1.000
z_{18}	0.235	1.000	0.487	0.839
z_{17}	0.305	0.388	0.300	0.496
z_{16}	0.781	0.931	1.000	0.741
z_{15}	0.197	0.578	0.194	0.165

3. Results

3.1. ECD data

Partial ECD mass spectra of all four isomers are shown in Fig. 1. Abundances of z_{15}, . . ., z_{19} ions were derived by summing up the intensities of all isotopic peaks in the cluster. The distinction between z, $z^{\bullet}$ and z' ions [32] was not made. All abundances in each spectrum were normalized by the most abundant z ion. The normalized data are given in Table 1.

3.2. MDS of gas-phase Trp-cage structures

Gas-phase structures of stereoisomers were markedly different from the "native" solution-phase conformation (Fig. 2). The number of neutral hydrogen bonds in the solution-phase structure was 9, while in the simulated gas-phase structures at room temperature it was between 15 and 16, consistent with

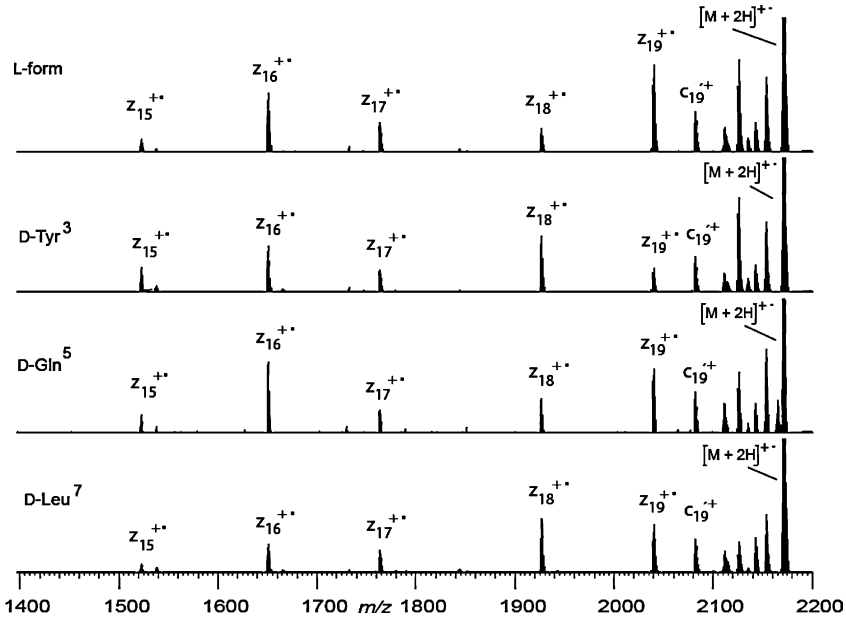

Fig. 1. Partial ECD mass spectra of dications of the four stereoisomers used in this work.

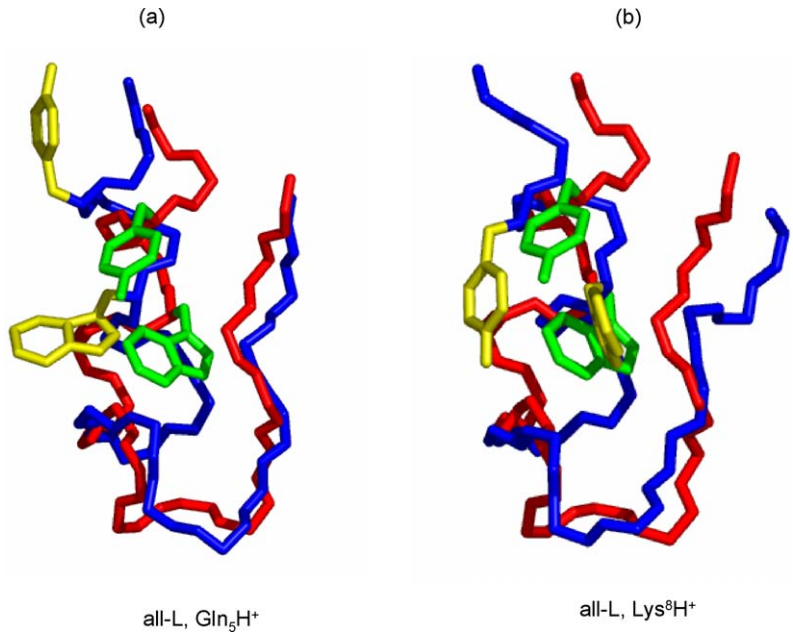

Fig. 2. Gas-phase structures of all-L Trp-cage dications (blue) calculated as the minimum-energy structures at 275 K shown in comparison (best fit) with the "native" solution-phase conformation determined by NMR [25]. The positions of the critical Tyr^3 and Trp^6 side chains are shown in yellow and green, respectively. (a) Gln^5-protonated, (b) Lys^8-protonated. The second proton is located on Arg^{16} in both cases. (For interpretation of the references to colour in this figure legend, the reader is referred to the web version of the article.)

the increased importance of hydrogen bonding and the loss of hydrophobic interactions in the gas phase. The average Δr value at 305 K for Gln^5-protonated dications was 0.39 nm, for all-L, 0.38 nm for D-Tyr^3, 0.43 nm for D-Gln^5 and 0.48 nm for D-Leu^7 stereoisomers. For Lys^8-protonated all-L dications, the Δr value was 0.44 nm, which may be one of the reasons why protonation of Gln^5 in the gas phase was more favorable. At 415 K, the corresponding Δr values changed by ca. 0.05–0.10 nm, indicating no global unfolding in the whole temperature range.

The Δr values computed for the global minimum structures were typically lower than the corresponding average values calculated for other bins than the global-minimum bin. This means that, despite the marked differences between the solution-phase and gas-phase structures, some general similarity between these structures was retained. Indeed, the transition from the solution-phase structure used as a starting point for the simulations to the stable gas-phase structure occurred directly and rapidly (5–7 ns, Fig. 3) without intermediate unfolding and refolding.

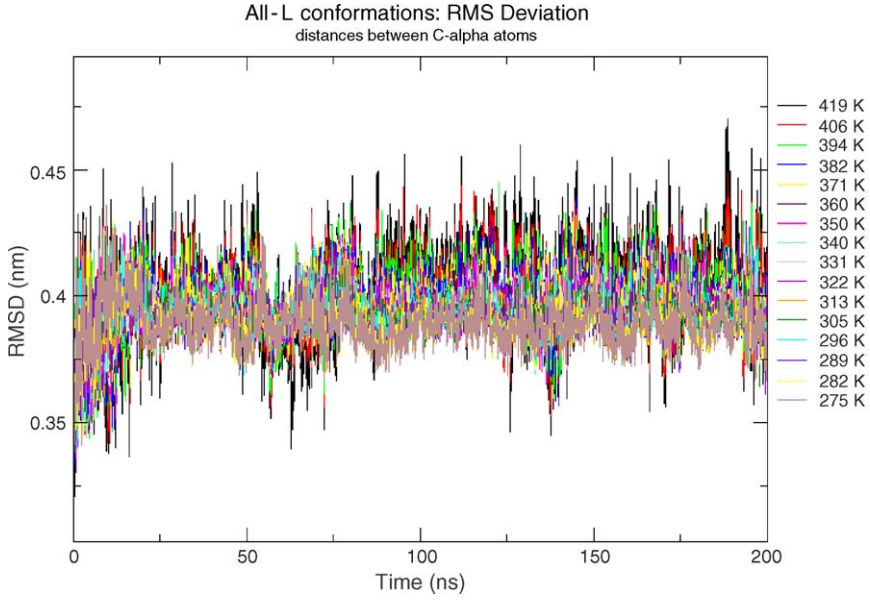

Fig. 3. MDS results obtained for the all-L Trp-cage dications. The time evolution of RMSD (average deviation from the initial structure) is shown. As initial structure (RMSD = 0; $t = 0$), the NMR-derived solution-phase structure was chosen. The plot shows smooth transition from the solution-phase structure to the gas-phase structure in 5–7 ns without intermediate unfolding and refolding, after which the gas-phase structure remains stable during the course of simulations (200 ns) in the whole temperature range.

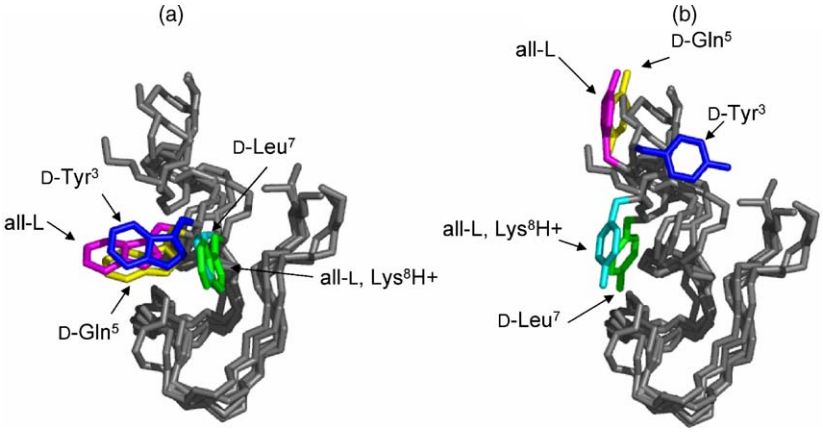

Fig. 4. Gas-phase structures of Trp-cage dications calculated as an average trajectory at 305 K shown in comparison (best fit) with each other. The positions of the critical Tyr^3 and Trp^6 side chains are shown in panels (a) and (b), respectively. Gln^5 residue was protonated if not indicated otherwise. The second proton is located on Arg^{16} in all cases.

The gas-phase structures of the studied stereoisomers were rather similar (Fig. 4): the average square-root deviation from the all-L dications was 0.11 nm for D-Tyr^3 and only 0.04 nm for D-Gln^5. The D-Leu^7 isomer differed the most, deviating from the all-L form by 0.29 nm. Change of the protonation site had a more significant effect that the stereo-inversion of the protonated Gln^5 residue: the average square-root deviations of the Lys^8-protonated all-L Trp-cage from the Gln^5-protonated all-L molecule was 0.16 nm.

Table 2 shows the simulated charge solvation pattern for the all-L stereoisomer at five different temperature points, providing the number of snapshots sampled every picosecond when the corresponding carbonyl established a hydrogen bond with the protonated Gln^5 side chain. Table 3 contains the 305 K data for three other stereoisomers and one all-L charge isomer. Only data for relevant carbonyls are shown, as well as for the Pro_{19} carbonyl at which charge solvation occurred most frequently.

Table 2
Simulation results for the all-L form of Trp-cage 2+ ions: the number of ps-long snapshots when a backbone carbonyl establishes a hydrogen bond with the protonated Gln^5 side chain (the other protonated residue is Arg^{16})

Temperature (K)	Asn^1	Leu^2	Tyr^3	Ile^4	Gln^5	Pro^{19}
275	35	0	0	38	0	67910
289	40	4	0	45	0	73447
305	95	7	0	95	0	77843
360	324	181	1	420	7	87934
419	1097	1030	8	917	85	87564

According to charge-solvation hypothesis, the Asn^1 column relates to z_{19} abundance in ECD mass spectra, Leu^2 column to z_{18}, etc.

Table 3
The same as in Table 2 but for three other stereoisomers and one all-L charge isomer and at the temperature of 305 K

	Asn^1	Leu^2	Tyr^3	Ile^4	Gln^5	Pro^{19}
D-Tyr^3	326	23	0	36	194	134356
D-Gln^5	7965	4261	1022	407	1462	58890
D-Leu^7	10573	1100	1	4519	71	44278
Lys^8H^+	–	8	689	987	138847	90300

This is not surprisingly, since in all global minimum structures the protonated Gln^5 side chain was solvated on the carbonyl-19. At the same time, the protonated Arg side chain was solvated on carbonyl-10 in all isomers except D-Leu^7. Additionally, $ArgH^+$ was solvated on carbonyl-12 in the D-Tyr^3 stereoisomer and Lys^8H^+ charge isomer. In the D-Leu^7 isomer, no charge solvation of the Arg side chain was present in the global minimum structure.

3.3. Testing the charge-solvation hypothesis

The comparison of the ECD mass spectra on Fig. 1 and the data in Tables 2 and 3 reveals several inconsistencies. First, the Pro_{19} carbonyl solvation exceeds that of the first five carbonyls by three orders of magnitude at room temperature and by two orders of magnitude at 419 K. Yet the abundance of the c_{19} ions is similar to that of the z_{15}, . . ., z_{19} fragments. Furthermore, the charge-solvation hypothesis predicts drastic temperature effect on the ECD patterns. This contradicts the experimental data showing that, while the abundances of z_{15}, . . ., z_{19} ions do become more similar at elevated temperatures, the effect is far gentler than predicted by Tables 2 and 3 [26].

Another inconsistency is the by two orders of magnitude larger frequencies of charge solvation in D-Gln^5 and D-Leu^7 isomers compared to two other stereoisomers. To test this prediction, the cross-section of producing z_{15}, . . ., z_{19} fragments for D-Gln^5 was compared with that of the isotopically labeled all-L isomer. The two stereoisomers were mixed in solution to 1:1 proportion and the dications of both species were isolated together and subjected to ECD. The relative cross-sections measured as the summed z_{15}, . . ., z_{19} fragment abundances normalized by the depletion of the precursor ions were for both stereoisomers indistinguishable within the 3% experimental error. Thus the other prediction of the charge-solvation model failed as well.

The 20 experimental z-ion abundances for all four stereoisomers (Table 1) were correlated with those predicted by MDS-based charge-solvation model for $T = 305$ K (Tables 2 and 3). This "global" correlation analysis between the experiment and

theory gave the correlation factor of $r = 0.425$. To interpret the statistical significance of this value, Monte Carlo simulations were performed in which the 20 abundances from Table 1 were correlated with 20 numbers randomly chosen in the 0, . . ., 1 interval. It was found that the 95% confidence level is attained at $r = 0.40$. Thus the observed global correlation between the ECD patterns and charge-solvation model predictions was statistically valid with a small margin.

However, when elevated-temperature MDS data were taken, the statistical significance of the correlation disappeared ($r = 0.115$ at 419 K). To test the ability of the charge-solvation model to recognize correct stereoisomers from their experimental, the experimental stereoisomer data were swapped between different stereoisomers (e.g., all-L data with D-Tyr^3 data), and for each new quartet of stereoisomers, global correlation with the unmixed MDS data was determined. The resulting correlations with each quartet of stereoisomers are presented in Fig. 5, where each isomer in a quartet is represented by a single letter: all-L by A, D-Tyr^3 by Y, D-Gln^5 by Q and D-Leu^7 by L. The best fit was found between AYQL (simulations) and LAYQ (experiment). Here, not a single isomer is recognized correctly. The three next-best candidates, QYLA, QAYL and LAQY, recognized correctly one stereoisomer each. The same result would be achieved on average by a random pick. The correct answer, AYQL → AYQL, gave a correlation factor below the average value for the 24 quartets, making the correct outcome less probable than a random pick. Thus the MDS predictions for charge-solvation model failed broadly the stereoisomer recognition test.

At a more detailed level, these predictions failed to account for the most significant effect of L → D substitution of the Tyr^3 residue, the dramatic change in the z_{19}/z_{18} abundance ratio [26].

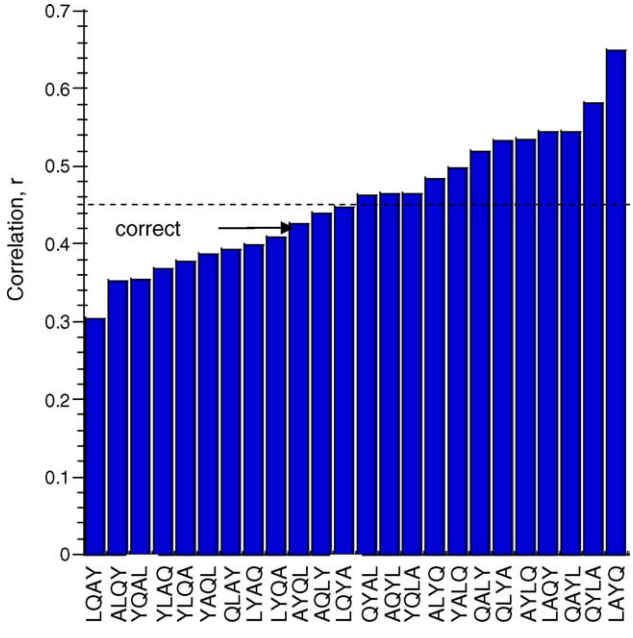

Fig. 5. The correlation factor r between the experiment and theory for charge-solvation model matched for different stereoisomer combinations. The solvation frequencies of protonated Gln^5 side chains by first five carbonyls in all-L (A), D-Tyr^3 (Y), D-Gln^5 (Q) and D-Leu^7 stereoisomers (L) (AYQL quartet) were compared with different quartet combinations of ECD data.

In contradiction with observations, continuing dominance of z_{19} fragments is predicted upon such substitution (compare Asn^1 and Leu^2 columns in Tables 2 and 3). Another prediction, the dominance of z_{15} over z_{16} for D-Gln^5, in also stark contrast with observations.

In the final test of the MDS predictions based on the charge-solvation hypothesis, the eventual systematic bias between the simulations and the experiment was removed by calculation, separately for these two groups of data, of the correlation factors between the patterns of different pairs of stereoisomers. For example, the experimental data were most similar between all-L and D-Gln^5 ($r = 0.900$), while in the charge-solvation MDS data the same pair was the most dissimilar ($r = 0.360$). In the experimental data, the most dissimilar pair was all-L and D-Tyr^3 ($r = -0.149$); the theory also predicted low degree of similarity for this pair ($r = 0.411$). Although four isomers give totally six pairs and thus six correlations, only four values will be statistically independent. Fig. 6 shows the correlation plot between the experimental and theoretical values for these four stereoisomer pairs. The overall correlation observed ($r = 0.326$) is not significant and is actually worse than the "global" correlation between the two full datasets. Thus the systematic bias between the experiment and theory is unlikely to be the major problem responsible for the poor fit between them.

Summarizing, the MDS predictions based on the charge-solvation hypothesis, despite demonstrating some degree of statistical validity, failed broadly to reproduce the observed in ECD abundances of N–C_α bond cleavages. The absolute predictions were off by several orders of magnitude, and the temperature effect was overestimated. Not only was the predictive power poorer than that of a random pick, but the predictions also missed the essential changes occurring in Trp-cage after L → D substitutions.

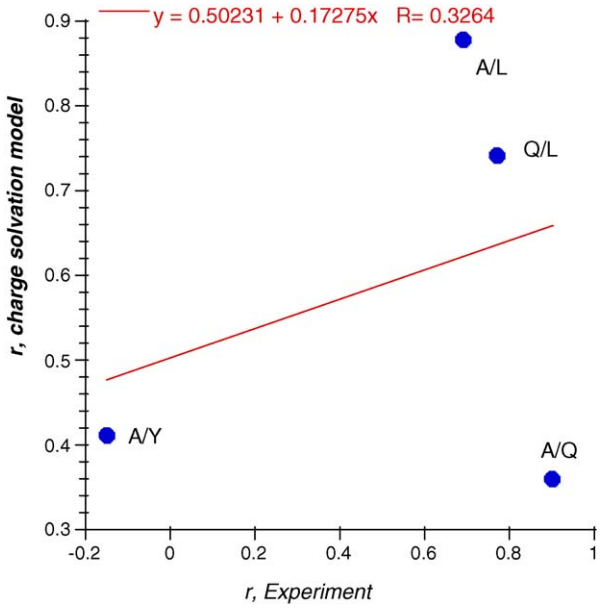

Fig. 6. The correlation for charge-solvation model between the experimental data and MDS after the systematic bias was removed (see text).

3.4. Elimination of possible sources of error

Three possible sources of error were considered: connected with the experiment, data interpretation and the simulations. To eliminate the possibility of an experimental error, all four stereoisomers of Trp-cage were synthesized anew. As already mentioned, the all-L isomer was also synthesized in the deuteriated form, which yielded z ions shifted by 6 Da. The experiments were performed not only with the standard water–methanol–acetic acid ESI solvent, but with two other solvents ammonium bicarbonate and quinhydrone. The electron energy was varied in the range ≈0–3 eV, and the duration of electron irradiation varied from 5 to 500 ms. Neither of these changes produced any significant variation in the ECD patterns. The correlation factor between z-ion abundances in any two spectra of the same isomer was >0.95. Thus the possibility of a gross experimental error was excluded.

The main error in data interpretation could come from a wrong assignment of the proton location. The alternative position of the neutralized proton is Lys^8, as in solution. Although the possibility of Lys^8 protonation in the gas phase dications has been excluded by ECD of trications [26], simulations of all-L Trp-cage for the charged Lys^8 and Arg^{16} residues were performed as additional negative control. Below 360 K, the simulations failed to give meaningful results, as Lys^8 was solvated mostly on Ile_4 carbonyl, predicting (Table 3) only z_{16} ions in the ECD mass spectrum. At 419 K, more carbonyls became involved in charge solvation, but the correlation with the ECD pattern remained negative ($r = -0.464$). Thus the alternative assignment of the protonation site was unlikely the cause of the problem.

Yet another error could arise if the N–C_α bond cleavages were induced not at the same amide that solvated the proton but the one N-terminal or C-terminal to that amide. To test this suggestion, the experimental data were shifted by ±1 residue (i.e., z_{19} ion abundances were compared with the charge-solvation probability on Tyr^3 and Asn^1 carbonyls instead of Leu^2 carbonyl). Such comparisons gave small anticorrelations (−0.109 and −0.325, respectively), a large drop compared to the unshifted value of 0.425. Thus "shifted" N–C_α fragmentation was not a problem, either.

The possibility that force-field MDS produces results poorly compatible with the actual experiments was also considered. The same program showed its adequacy in a number of other studies, e.g., for much larger villin headpiece [33]. Furthermore, gas-phase fluorescence experiments showed stability of 2+ ions of all-L Trp-cage up to 420 K, in line with the simulations [34].

Generally, empirical MDS algorithms are less suited for quantitative predictions of charge solvation than ab initio approaches, although polarization effects are accounted for in the used force field. But no inconsistency in the MDS results was found in the current study: charge solvation frequencies showed smooth behavior at different temperatures for all carbonyls (Table 2 for all-L isomer; other data behave similarly). The frequencies become more equal as temperature increases, in line with the theoretical expectations and experimental results [26]. Thus MDS should reproduce at least coarse features arising due to L → D substitution.

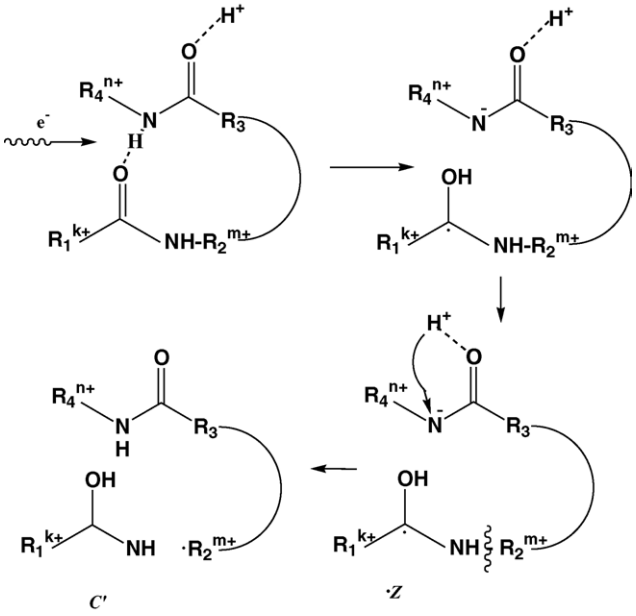

Scheme 1. The suggested N–C_α bond cleavage mechanism in ECD.

3.5. Alternative ECD mechanism

In view of the failure of the MDS predictions based on the charge-solvation model, the following new ECD mechanism is considered (Scheme 1). The low-energy electron is captured on a neutral hydrogen bond between a backbone nitrogen atom and another backbone carbonyl (such bonds are found in α-helixes and β-sheets). The main considered case is the N–H···O=C type bonding (Scheme 1), although in principle any neutral hydrogen bonding to a carbonyl is suitable. Following the electron capture by the N–H···O=C group, an anionic site is formed at the nitrogen atom, and simultaneously hydrogen atom is transferred to the carbonyl which forms labile aminoketyl radical:

$$\text{N–H} \cdots \text{O=C} + \text{e}^- \rightarrow \text{N}^- + {}^\bullet\text{C(OH)} \quad (1)$$

The N–C_α bond in the aminoketyl radical then fragments as in the "classical" hydrogen-atom mechanism [13]. Once the aminoketyl radical is formed, such a cleavage is almost thermoneutral [15–17]. Then the most loosely bound ionizing proton neutralizes the amide anion via an appropriate intra-molecular proton transfer [35].

This mechanism in Scheme 1 predicts that the frequencies of N–C_α bond cleavage are proportional to the probability of neutral hydrogen bonding to the corresponding carbonyl. To test this prediction, the pattern of neutral hydrogen bonding involving each of the carbonyls was examined. Table 4 show the numerical results for neutral hydrogen bonding patterns at five temperature points simulated for the all-L stereoisomer. Table 5 shows 305 K data for the remaining three stereoisomers and one charge isomer. The data represent the percentage of time when the corresponding carbonyl establishes a neutral hydrogen bond with any other part of the molecule.

A brief look at Tables 4 and 5 reveals that the data there are mostly free from the problems encountered by the MDS

Table 4
Simulation results for the Gln[5]-protonated all-L form of Trp-cage 2+ ions (the other protonated residue is Arg[16]): percentage of time when a backbone carbonyl establishes a neutral hydrogen bond with any other part of the molecule

Temperature (K)	Asn[1]	Leu[2]	Tyr[3]	Ile[4]	Gln[5]	Pro[19]
275	89.8	53.9	17.3	64.8	31.1	96.8
289	89.1	51.9	18.3	62.9	29.6	95.9
305	87.8	50.5	19.2	60.9	28.3	95.5
360	82.7	46.8	24.2	55.9	26.0	94.8
419	72.6	47.1	33.0	53.3	25.7	78.3

results based on the charge-solvation hypothesis. The Pro_{19} anomaly does not exist, and the second difficulty of the charge-solvation model, vastly different solvation probabilities on the same carbonyls for different stereoisomers, also disappeared. The frequencies of H-bonding change with temperature only modestly (Table 4 for all-L; data for other isomers behave similarly), in line with observations. Finally, the ratio of the contents in Asn[1] and Leu[2] columns reverses for D-Tyr[3] compared to all-L (compare first two columns in Tables 4 and 5), similar to the behavior of the z_{19}/z_{18} ratio in the mass spectra ([26]; Fig. 1). The chiral recognition factor for D-Tyr[3] [26] calculated from the MDS data is 2.6, in a qualitative agreement with the value of 10.5 for experimental data.

Quantification of the theory/experiment similarities confirmed these qualitative findings. A statistically significant "global" correlation was found ($r = 0.677$, $P > 99.5\%$) with the frequency of establishing at least one neutral hydrogen bond at 305 K. At $T = 419$ K, the correlation slightly increased to 0.680, and it vanished as expected when the 305 K experimental data were shifted by ±1 residue ($r = -0.014$ and -0.181, respectively).

To test the stereoisomer recognition ability of this hypothesis, the experimental stereoisomer data were mixed and for each new quartet, correlation with the unmixed MDS data was determined, as it was done previously for the charge-solvation hypothesis. The results (Fig. 7) showed that the new model favors the correct quartet, AYQL. The three next-best quartets, ALQY, QYAL and QYLQ, correctly recognize two stereoisomers each (three is impossible), confirming that the perfect match AYQL → AYQL was not a random event. In the final test similar to that shown in Fig. 6, an excellent correlation ($r = 0.972$) was obtained between the theory and experiment upon removing the systematic bias between them (Fig. 8). This correlation has improved compared to the direct "global" comparison, indicating that a refinement of the calculations and reduction of the bias can bring the predicted ECD abundances even closer to the experiment.

Table 5
The same as in Table 4 but for one temperature point (305 K), three stereoisomers and one charge isomer

	Asn[1]	Leu[2]	Tyr[3]	Ile[4]‘	Gln[5]	Pro[19]
D-Tyr[3]	57.6	87.0	85.9	65.1	13.0	N/A
D-Gln[5]	72.5	58.8	39.8	54.5	29.9	N/A
D-Leu[7]	68.8	71.9	53.3	49.7	30.4	52.1
Lys^8H^+	65.3	49.8	74.7	44.1	73.4	N/A

N/A—data were not calculated.

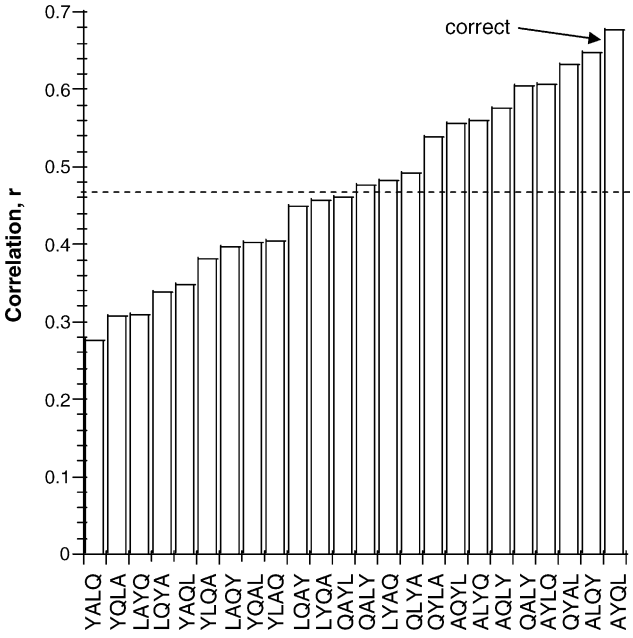

Fig. 7. The same as in Fig. 5 but for the neutral hydrogen bonding model.

3.6. Bond duration versus bond creation rate

The above results strongly support the role of neutral hydrogen bonding in the ECD mechanism. They also support the validity of the MDS results for describing the neutral hydrogen bonding pattern. What remains to be found is whether the N–C_α bond cleavage frequency is directly proportional to that of the neutral H-bonding as in Scheme 1, or rather to the frequency of creation/destruction of such bonding. The latter process is one of the ways of vibrational energy transfer between different parts of the molecule. The amide undergoing a higher rate of H-bond creation/destruction experiences also a larger energy flow

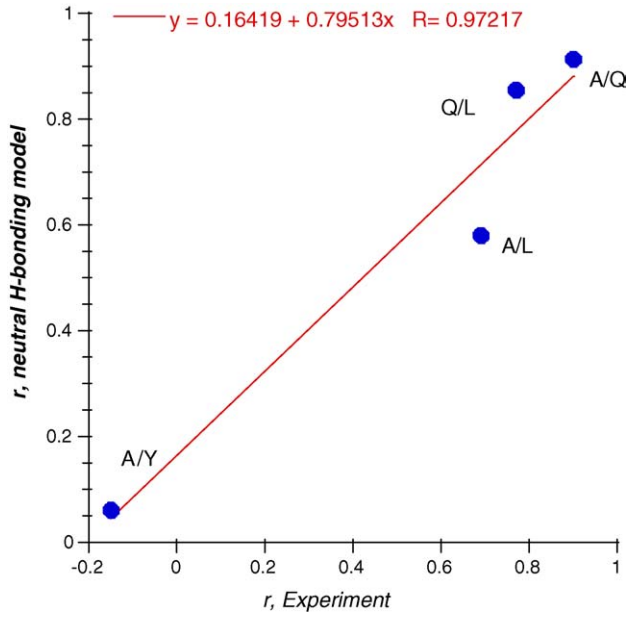

Fig. 8. The same as in Fig. 6 but for the neutral hydrogen bonding model.

Table 6
The normalized frequencies of: creation-disruption of an H-bond by a given carbonyl/existence of a single neutral hydrogen bond/existence of two neutral hydrogen bonds to the same carbonyl

Carbonyl	all-L, simulations	D-Tyr[3], simulations	D-Gln[5], simulations	D-Leu[7], simulations
Asn[1]	1.000/0.986/1.000	0.865/0.649/0.170	1.000/1.000/1.000	0.856/1.000/0.570
Leu[2]	0.840/0.873/0.141	0.563/1.000/0.041	0.943/0.830/0.607	1.000/0.903/1.000
Tyr[3]	0.564/0.395/0.085	0.697/0.983/0.698	0.724/0.616/0.228	0.944/0.706/0.599
Ile[4]	0.888/1.00/0.226	1.000/0.759/1.000	0.845/0.905/0.293	0.782/0.749/0.185
Gln[5]	0.563/0.539/0.006	0.490/0.210/0.104	0.691/0.597/0.126	0.740/0.502/0.214

through that amide and thus may fragment at a higher rate. To test whether the energy transport or the H-bonding itself affect the rate of N–C_α bond cleavages, the normalized frequencies of H-bonds creation/disruption of each of the carbonyls were calculated (Table 6) and the correlation of these values with z-fragment abundances was determined. The value of the correlation ($r = 0.445$) was comparable with the "global" correlation value for the charge-solvation model and, although statistically significant, was much lower than that for the total H-bonding mechanism. It is however hard to completely disentangle the bond creation rates (first numbers in Table 6) and the total bond duration (Tables 4 and 5), as their values correlated statistically ($r = 0.650$). But based on the much better correlation with the experimental data, the mechanism in Scheme 1 is preferred over the energy transport mechanism.

As an additional support to Scheme 1, total durations were determined separately for single and double hydrogen bonds to a given carbonyl (second and third values in Table 6). These frequencies correlated strongly with z-ion abundances: $r = 0.616$ for single H-bonding and $r = 0.515$ for double H-bonding. The conclusion was therefore confirmed that the H-bonding itself and not the rate of its establishing determines the N–C_α bond cleavage probabilities.

4. Discussion

Similar to the models of Simons and co-workers [12] as well as Syrstad and Tureček [36], the mechanism in Scheme 1 avoids direct neutralization of the positive site and assumes instead electron capture by a neutral group. The suggested mechanism has however the following advantages. The $-N^-$-anion, being an even-electron entity in the ground electronic state, is more stable and less mobile that the electronically excited radical amide anions in other models. The N–C_α bond cleavage competition with radiative and non-radiative relaxation of the electronically excited state is also avoided in Scheme 1. While the overall exothermicity after bond cleavage and energy relaxation is the same in all mechanisms, capture on the neutral N–H···O=C hydrogen bond is more energetically favorable than electron capture on the electronically excited state of carbonyl. Indeed, (1) can be presented as successive steps of: (1) breakage of the H-bonding (≈−0.2 eV [37]), abstraction of H^+ from –NH– (−15.5 eV [38]), recombination of H^+ and e^- to $H^\bullet$ (+13.6 eV) and $H^\bullet$ attachment to the carbonyl (+0.6 eV [15,16]). The balance is ≈−1.5 eV, which makes (1) by ≈1 eV less endothermic than the capture on the π* C=O orbital [12]. Furthermore, abstraction by a radical anion of a proton from a neutral group [36] is replaced by an intra-molecular proton transfer. The latter process has a smaller barrier and thus occurs faster. Coulombic attraction assists (1) to the same degree as in other mechanisms.

The charge recombination ($-N^-$ and a proton) can occur in Scheme 1 after the N–C_α bond cleavage, but before fragment separation. The least basic proton is most likely to participate in the recombination, in agreement with the observation that the least basic protonated site disappears in ECD [26]. The recombination process is hugely exothermic (6–8 eV), and can be the driving force for the fragment separation. Indeed, the 15–16 neutral H-bonds in Trp-cage dications represent together 3.0–3.5 eV of binding energy, to which <1 eV should be added to account for the solvation of the remaining charge on the complementary fragment. What remains to be explained is how the ≈1.5 eV barrier for electron capture on the H-bond can be overcome.

The electron may obtain the required 1.5 eV of the kinetic energy from the potential energy of the electrostatic field of the dications. In multiply-protonated peptides, every new charge increases this energy by on average ≈1.1 eV [39]. Thus the kinetic energy gained by an electron resting at infinity and attracted by a doubly protonated peptide is ca. 2.2 eV, which is enough for the mechanism in Scheme 1 but not for capture on the excited state of the carbonyl [12]. Given the average nature of this figure, most of peptide's N–C_α bonds will be accessible for cleavage to zero-energy electrons. This result is in a qualitative agreement with the observed cleavage efficiency for doubly charged peptides, and is certainly in agreement for Trp-cage dications for which only 38% of possible N–C_α cleavages are observed. Note that in ECD of 3+ Trp-cage ions, all possible N–C_α cleavages are present [26]. However, with sub-zero-energy electrons as in electron transfer dissociation (ETD), N–C_α bond fragmentation in doubly charged peptides should be limited, as indeed found in experiments [3].

The role of the neutral hydrogen bonding in ECD is two-fold. On the one hand, multiple H-bonding in the molecule prevents fragment separation, thus inhibiting the observation of N–C_α bond cleavages [22]. This feature has been used to derive "melting temperature" data on different charge states of gas-phase ubiquitin [24]. On the other hand, in MALDI in-source decay (ISD), a single H-bond to a carbonyl promotes N–C_α cleavage next to that carbonyl [40,41]. McLafferty et al. have found that the maximum of N–C_α cleavage frequency in α-helical ubiquitin 13+ ions is shifted 3–4 residues away from the assumed protonated site [42]. This distance roughly corresponds to one

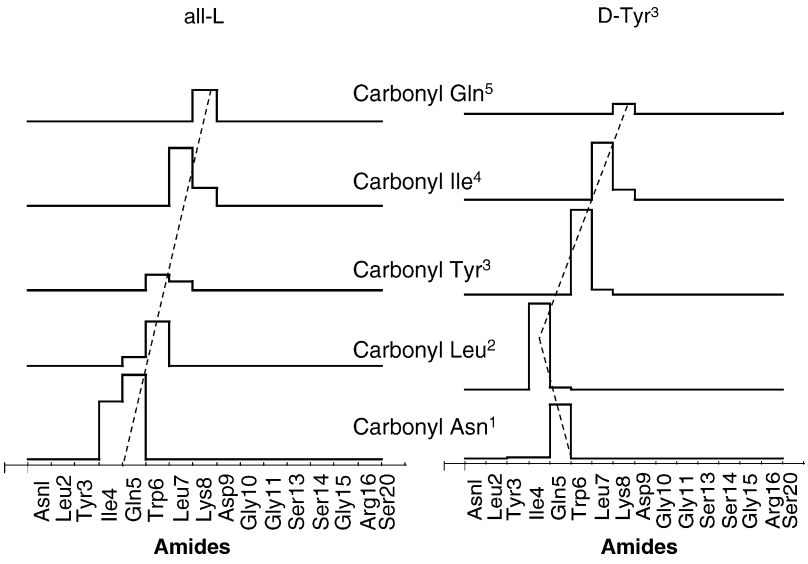

Fig. 9. The relative frequencies of establishing neutral hydrogen bonding between first five N-terminal carbonyls and backbone amides of other residues in: all-L isomer (left) and D-Tyr^3 isomer (right).

turn of the α-helix. The N-terminal part of the Trp-cage is also α-helical [25]. The left panel of Fig. 9 presents the relative frequencies of establishing neutral hydrogen bonding between the first five N-terminal carbonyls and the backbone amides of other residues in all-L Trp-cage. The α-helical character (3–4 residue shift) is obvious in the bonding pattern: while the carbonyl of Asn^1 preferentially establishes H-bonding with the amides of Ile^4 and Gln^5, the carbonyl of Gln^5 forms H-bonds with the Lys^8 amide. Thus according to Scheme 1, formation of z_{19} to z_{15} ions is caused by electron capture on amides of residues Ile^4 through Lys^8, respectively. This is a region largely located between the two charges present at Gln^5 and Arg^{16} (the latter charge is solvated on carbonyl-10). Thus there is a large potential coulombic energy in that region, which should promote an efficient, exothermic electron capture on the backbone amides.

In D-Tyr^3 Trp-cage (Fig. 9, right panel), disruption of the α-helix occurs in the first two residues. Compared to the all-L isomer, the frequency of hydrogen bonding in D-Tyr^3 Trp-cage drops for the first carbonyl and increases for the second carbonyl—the feature reflected in the changed abundances of z_{19} and z_{18} ions (Fig. 1). This disturbance is localized to the region adjacent to the L → D substitution—and so is the effect of such substitution on ECD cleavages [28]. Thus the H-bonding model easily accounts for the sensitivity of ECD to L → D substitution. This sensitivity was previously difficult to explain given the identical chemical properties of amino acid stereoisomers, and the small effect of chiral substitution on the overall gas-phase structure (see Fig. 4). The neutral H-bonding is rather insensitive to temperature: the average for five carbonyls percentage of time of involvement in neutral H-bonding for the all-L isomer is 51.4% at 275 K, 48.5% at 322 K and 46.3% at 419 K. Such a modest effect is in stark contrast with the exponential temperature sensitivity of charge solvation (Table 2), and it is in agreement with the experimentally observed by McLafferty et al. relative insensitivity of ECD patterns to changes in electron energy and ionic temperature [42]. The main effect of an elevated temperature is that H-bonding becomes more evenly distributed among different carbonyls as the molecule accesses more conformations and the system becomes more chaotic. A similar effect has also been noticed for the abundances of ECD fragments of Trp dications: the values become more similar, and the chiral recognition diminishes [26]. Conversely, at low temperatures hydrogen bonding pattern converges to a few dominant bonds. This explains why ECD fragment abundances show reduced trends with a temperature increase [42], and why at 86 K only two fragments are present in the ECD mass spectrum of substance P dications [43].

Do the presented data completely dismiss the charge-solvation model of N–C_α bond cleavage in ECD? We do not think so. Despite the success of the neutral hydrogen bonding hypothesis in fitting the MDS results and the relative failure in that task of the charge-solvation model, the role of charge in ECD is supported by a range of other experimental observations. For instance, abundant evidence is present in the $(M - X^{\bullet})$ region of ECD mass spectra [44–46] for losses in the charge-reduced species from the side chains involved in either protonation or charge solvation. It is also hard to easily dismiss the fact that electron attachment to a positive charge is by far more exothermic than attachment to any neutral group. It appears likely that both neutral H-bonding and charge solvation determine the backbone cleavage probabilities in ECD.

What however is clear from the current study is that the charge-solvation model may be less helpful in predicting the ECD fragment abundances than the mechanism in Scheme 1. Whether this is a consequence of the inadequacy of the modern force-field approximations for quantitative prediction of charge solvation patterns, is an open question. We are of the opinion that it would be too extreme to simply dismiss the MDS results citing potential problems in the empirical force fields. Force-field MDS is the basis of the extensive studies of gas-phase polypeptide molecules and ions [e.g., 47,48], where arrival to the correct lowest-energy structure by MDS is critical. For instance, in ref.

[47] it was found that unsolvated, uncharged alanine-based peptides may have β-sheet structures, while in a protonated state they may accept α-helical or globular conformation. Thus charge was found more than anything else to control the gas-phase structure. In ref. [48], gas-phase structures of short peptides provided by AMBER force field modeling were linked to their biological activity. Having cited these examples, we admit that it is quite possible that further improvements in the force-field potentials can bring the predictions based on the charge-solvation model closer to the ECD results.

The mechanism in Scheme 1 was called to existence by the necessity to explain the obtained MDS results. It finds support in thermodynamics and in a number of other observations, as discussed above. Although good correlation between the theory predictions and the experiment is a necessary condition for any scientific hypothesis, the presence of such a correlation by itself does not guarantee the correctness of the hypothesis. Thus the mechanism in Scheme 1 may not be the last word. It needs further validation and thorough testing. It will however remain an important step that highlighted the role of neutral hydrogen bonding—the role that has so far been largely ignored by other mechanisms.

5. Conclusions

Comparison between the experiment and theory for four Trp-cage stereoisomer dications revealed inadequacy of the MDS-based predictions made with the charge-solvation hypothesis that explicitly assumes the N–C_α bond cleavage in the vicinity of a charged site. A statistical link between the charge position and the site of preferred cleavage is present but weaker than expected, which summarily precludes meaningful predictions of ECD fragment abundances based on charge solvation pattern obtained with currently available force-field MDS algorithms. Whether this failure is due to the problems in the force-field MDS, the charge-solvation hypothesis itself or other factors is not totally clear, but that appears unlikely that this result is entirely due to MDS.

Another finding is the strong correlation present between the frequencies of neutral hydrogen bonding obtained by MDS and experimentally observed N–C_α bond cleavage frequencies. This finding strongly supports the role of such bonding in ECD, e.g., as depicted in Scheme 1. The predictive power of the neutral H-bonding model was tested in this work and found satisfactory. The model was capable to explain the relative abundances of the observed z ions and even predict the changes arising in ECD patterns due to L → D substitutions. All four stereoisomers could be correctly identified by comparing experimental and theoretical data.

These findings do not mean complete dismissal of the charge-solvation hypothesis, although a certain paradigm shift in understanding the mechanism of ECD seems unavoidable. Future efforts should reveal the interplay between the charged and neutral hydrogen bonding for refining the predictions of the ECD fragment abundances and for better relating them to protein gas-phase structures, with the final goal of solving these structures.

Acknowledgements

The non-deuteriated all-L and D-Tyr^3 Trp-cage stereoisomers were synthesized and purified by Åke Engström; others were produced by Marina Zoubareva. This work was supported by the Knut and Alice Wallenberg Foundation and Wallenberg Consortium North (grant WCN2003-UU/SLU-009 to RZ) as well as the Swedish Research Council (grants 621-2004-4897 and 621-2003-4877 to RZ).

References

[1] R.A. Zubarev, N.L. Kelleher, F.W. McLafferty, J. Am. Chem. Soc. 120 (1998) 3265.
[2] J.B. Fenn, M. Mann, S.F.W. Chin Kai Meng, C.M. Whitehouse, Science 246 (1989) 64.
[3] J.E.P. Syka, J.J. Coon, M.J. Schroeder, J. Shabanowitz, D.F. Hunt, Proc. Natl. Acad. Sci. U.S.A. 101 (2004) 9528.
[4] F.W. McLafferty, in: C.J. McNeal (Ed.), Mass Spectrometry in the Analysis of Large Molecules, John Wiley, New York, 1986, p. 107.
[5] S.B. Nielsen, J.U. Andersen, P. Hvelplund, T.J.D. Jorgensen, M. Sorensen, S. Tomita, Int. J. Mass Spectrom. 213 (2002) 225.
[6] A.S. Misharin, O.A. Silivra, F. Kjekdsen, R.A. Zubarev, Rapid Commun. Mass Spectrom. 19 (2005) 2163.
[7] Y. Ge, M. ElNaggar, S.K. Sze, H.B. Oh, T.P. Begley, F.W. McLafferty, H. Boshoff, C.E. Barry III, J. Am. Soc. Mass Spectrom. 14 (2003) 253.
[8] F. Kjeldsen, K.F. Haselmann, B.A. Budnik, E.S. Sørensen, R.A. Zubarev, Anal. Chem. 75 (2003) 2355.
[9] M.L. Nielsen, M.M. Savitski, R.A. Zubarev, Mol. Cell. Proteomics 6 (2005) 835.
[10] M.J. Chalmers, K. Håkansson, R. Johnson, R. Smith, J. Shen, M.R. Emmett, A.G. Marshall, Proteomics 4 (2004) 970.
[11] R.R. Hudgins, K. Hakansson, J.P. Quinn, C.L. Hendrickson, A.G. Marshall, Proceedings of the 50th Annual Conference on Mass Spectrometry and Allied Topics, Orlando, FL, June, 2002.
[12] M. Sobczyk, I. Anusiewicz, J. Berdys-Kochanska, A. Sawicka, P. Skurski, J. Simons, J. Phys. Chem. A 109 (2005) 250.
[13] R.A. Zubarev, N.A. Kruger, E.K. Fridriksson, M.A. Lewis, D.M. Horn, B.K. Carpenter, F.W. McLafferty, J. Am. Chem. Soc. 121 (1999) 2857.
[14] N. Leymarie, C.E. Costello, P.B. O'Connor, J. Am. Chem. Soc. 125 (2003) 8949.
[15] R.A. Zubarev, K.F. Haselmann, B.A. Budnik, K. Kjeldsen, F. Jensen, Eur. J. Mass Spectrom. 8 (2002) 337.
[16] F. Tureček, J. Am. Chem. Soc. 125 (2003) 5954.
[17] V. Bakken, T. Helgaker, E. Uggerud, Eur. J. Mass Spectrom. 10 (2004) 625.
[18] K.F. Haselmann, T.J.D. Jørgensen, B.A. Budnik, F. Jensen, R.A. Zubarev, Rapid Commun. Mass Spectrom. 16 (2002) 2260.
[19] N.C. Polfer, Structural elucidation of peptides and proteins by Fourier transform ion cyclotron resonance mass spectrometry, Ph.D. Thesis, University of Edinburgh, Edinburgh, UK, 2003.
[20] N.C. Polfer, K.F. Haselmann, P.R.R. Langridge-Smith, P. Barran, Mol. Phys. 103 (2005) 1481.
[21] I.A. Kaltashov, S.J. Eyles, Mass Spec. Rev. 21 (2002) 37.
[22] R.A. Zubarev, E.K. Fridriksson, D.M. Horn, N.L. Kelleher, N.A. Kruger, B.K. Carpenter, F.W. McLafferty, Anal. Chem. 72 (2000) 563.
[23] P.A. Sullivan, J. Axelsson, S. Altmann, A.P. Quist, B.U.R. Sunqvist, C.T. Reimann, J. Am. Soc. Mass Spectrom. 7 (1996) 329.
[24] K. Breuker, H.B. Oh, D.M. Horn, B.A. Cerda, F.W. McLafferty, J. Am. Chem. Soc. 124 (2002) 6407.
[25] J.W. Neidigh, R.M. Fesinmeyer, N.H. Andersen, Nat. Struct. Biol. 9 (2002) 425.
[26] C. Adams, B.A. Budnik, K.F. Haselmann, F. Kjeldsen, R.A. Zubarev, J. Am. Soc. Mass Spectrom. 15 (2004) 1087.
[27] G. Kreil, Science 266 (1994) 996.
[28] C. Adams, R.A. Zubarev, Anal. Chem. 77 (2005) 4571.

[29] C. Zhao, T.D. Wood, S. Bruckenstein, J. Am. Soc. Mass Spectrom. 16 (2005) 409.
[30] E. Lindahl, B.A. Hess, D. van der Spoel, J. Mol. Mod. 7 (2001) 306.
[31] B. Hess, H. Bekker, H.J.C. Berendsen, J.G.E.M. Fraaije, J. Comput. Chem. 18 (1997) 1463.
[32] R.A. Zubarev, Mass Spectrom. Rev. 22 (2003) 57.
[33] D. van der Spoel, E. Lindahl, J. Phys. Chem. B 7 (2003) 11178.
[34] A.T. Iavarone, J.H. Parks, J. Am. Chem. Soc. 125 (2005) 8606.
[35] A.M. Kuznetsov, J. Ulstrup, Chem. Phys. 188 (1994) 131.
[36] E.A. Syrstad, F. Tureček, J. Am. Soc. Mass. Spectrom. 16 (2005) 208.
[37] A.T. Hagler, P. Dauber, S. Lifson, J. Am. Chem. Soc. 101 (1979) 5111.
[38] F. Kjeldsen, O.A. Silivra, I.A. Ivonin, K.F. Haselmann, M. Gorshkov, R.A. Zubarev, Chem. Eur. J. 11 (2005) 1803.
[39] B.A. Budnik, Y.O. Tsybin, P. Håkansson, R.A. Zubarev, J. Mass Spectrom. 37 (2002) 1141.
[40] P.J. Calba, J.F. Muller, M. Inouye, Rapid Commun. Mass Spectrom. 12 (1998) 1727.
[41] T. Kocher, A. Engstrom, R.A. Zubarev, Anal. Chem. 77 (2005) 172.
[42] K. Breuker, H.B. Oh, C. Lin, B.K. Carpenter, F.W. McLafferty, Proc. Natl. Acad. Sci. U.S.A. 101 (2004) 14011.
[43] R. Mihalca, A.J. Kleinnijenhuis, L.A. McDonnell, A.J.R. Heck, R.M.A. Heeren, J. Am. Soc. Mass Spectrom. 15 (2004) 1869.
[44] H.J. Cooper, R.R. Hudgins, K. Hakansson, A.G. Marshall, J. Am. Soc. Mass Spectrom. 13 (2002) 241.
[45] K.F. Haselmann, N.C. Polfer, B.A. Budnik, F. Kjeldsen, R.A. Zubarev, J. Mass Spectrom. 8 (2002) 461.
[46] H.J. Cooper, K. Håkansson, A.G. Marshall, R.R. Hudgins, K.F. Haselmann, F. Kjeldsen, B.A. Budnik, N.C. Polfer, R.A. Zubarev, Eur. J. Mass Spectrom. 8 (2002) 461;
H.J. Cooper, K. Håkansson, A.G. Marshall, R.R. Hudgins, K.F. Haselmann, F. Kjeldsen, B.A. Budnik, N.C. Polfer, R.A. Zubarev, Eur. J. Mass Spectrom. 9 (2003) 221.
[47] P. Dugourd, R. Antoine, G. Breaux, M. Broyer, M.F. Jarrold, J. Am. Chem. Soc. 127 (2005) 4675.
[48] P.E. Barran, N.C. Polfer, D.J. Campopiano, D.J. Clarke, P.R.R. Langridge-Smith, R.J. Langley, J.R.W. Govan, A. Maxwell, J.R. Dorin, R.P. Millar, M.T. Bowers, Int J. Mass Spectrom. 240 (2005) 273.